Article:
Li, Y orcid.org/0000-0002-4980-1592, Borbely, M and Bell, A orcid.org/0000-0002-2061-3862 (2021) The Influence of Oxygen Vacancies on Piezoelectricity in Samarium-Doped Pb(Mg1/3Nb2/3)O3-PbTiO3 Ceramics. Journal of the American Ceramic Society, 104 (6). pp. 2678-2688. ISSN 0002-7820

https://doi.org/10.1111/jace.17619

MISS YANG LI (Orcid ID : 0000-0002-4980-1592)

PROFESSOR ANDREW JOHN BELL (Orcid ID : 0000-0002-2061-3862)

Article type : Article

The Influence of Oxygen Vacancies on Piezoelectricity in Samarium-Doped $Pb(Mg_{1/3}Nb_{2/3})O_3$-$PbTiO_3$ Ceramics

Yang Li, Marcell Borbely, Andrew Bell*

School of Chemical and Process Engineering, Faculty of Engineering,

University of Leeds, Leeds, U.K.

*Corresponding Author: a.j.bell@leeds.ac.uk

Abstract

A study of $0.71Pb(Mg_{1/3}Nb_{2/3})O_3$-$0.29PbTiO_3$ shows that, when it is doped with 2.5% Sm on the A-site, in addition to an almost 3-fold increase in piezoelectric charge coefficient and dielectric permittivity, there is a 2 order of magnitude reduction in conductivity, attributed to a decrease in oxygen vacancy concentration. An analysis of the nonlinearity of permittivity with respect to field amplitude shows that both the reversible and irreversible contributions increase significantly with Sm-doping, with simple models showing that these changes are consistent with a reduction in the concentration of dipolar defects that can inhibit both polarization rotation and domain wall translation. Contrary to the argument that doping increases heterogeneity, there is little change in the diffuseness of the peak in permittivity as a function temperature, whilst there is a 15% increase in spontaneous polarization with Sm addition. Through comparison of the Rayleigh law parameters with those published for other piezoelectric materials, it is concluded that a significant contribution to the observed increase in piezoelectric performance due to Sm-doping of PMN-PT

This article has been accepted for publication and undergone full peer review but has not been through the copyediting, typesetting, pagination and proofreading process, which may lead to differences between this version and the Version of Record. Please cite this article as doi: 10.1111/JACE.17619

is similar in origin to that seen in soft, donor-doped PZT and other conventional piezoelectric ceramics.

Keywords: piezoelectricity, ferroelectricity; domains ; oxygen vacancies

Introduction

$Pb(Mg_{1/3}Nb_{2/3})O_3$-$PbTiO_3$ (PMN-PT) [1, 2] is a key material for understanding the interaction between the chemical disorder, the competing long-range polar structural symmetries that define the morphotropic phase boundary (MPB) and the mechanism that provides giant electromechanical coupling. PMN-PT single crystals, which exhibit the largest piezoelectric coefficients ($d_{33} \approx 2000$ pC/N) around the MPB,[3-6] are now the primary choice for a number of piezoelectric applications, including naval sonar and medical ultrasound imaging. To meet the tailored performance requirements of piezoelectric devices, much effort has been focused on the impact of aliovalent ion doping on the piezoelectric response of ferroelectrics.[7-9] In relaxor based systems, it is reported that rare-earth dopants can introduce effective random fields and bonds and/or change the ordering degree of B-site cations. Dopants can also influence the domain size, dielectric properties and diffuseness of the phase transition.[8] In particular, for PMN-PT, it has been reported that rare earth elements samarium (Sm) and ytterbium (Yb) doping could contribute to a high dielectric permittivity.[10-12]

Recently, Li et al.[10, 11] successfully achieved an ultrahigh d_{33} of up to 4000 pC/N in Sm-doped PMN-PT single crystals and 1500 pC/N in ceramics. However, the associated reduction in Curie temperature (T_C) to 85~110˚C, may limit its practical application. An optimized d_{33} of 910 pC/N with a high T_C = 184˚C was obtained in Sm-doped $Pb(Mg_{1/3}Nb_{2/3})O_3$-$PbZrO_3$-$PbTiO_3$ (PMN-PZT) ternary system.[13] It has been proposed that Sm introduces increased local structural heterogeneity to modify the interfacial energy between polar nanoregions or structural fluctuations and further flattens the free energy landscape, producing a superior piezoelectric response. It is suggested that the aliovalent Sm^{3+} is an effective way to enhance relaxor behavior and therefore increases the dielectric permittivity.[13] A first principles calculation was explored to explain the high d_{33} at an atomic scale, which reveals that Sm^{3+} with a small ionic size and a high valence will occupy the A-site in PMN-PT and lead to a large local structural variation, produce local structural heterogeneity.[14] It has also been concluded that Sm-doping of PMN-PT leads to an increase in the concentration of oxygen vacancies, which in turn produces the structural-polar heterogeneity and improves piezoelectric response.[15] However, this increase of oxygen vacancies concentration is contrary with the conventional view of donor dopant effects in Pb-based perovskites. As reported, Sm doping can significantly raise the dielectric, ferroelectric and piezoelectric properties in $Pb(Zr,Ti)O_3$ (PZT) ceramics due to a reduction in oxygen vacancy concentration, leading to an enhancement of domain wall motion.[16-18]

In conventional piezoelectric ceramics, such as PZT, the impact of dopants is most often discussed in terms of changes to the domain wall contributions to piezoelectric properties. It is said that the concentration of polar defect pairs (usually oxygen vacancies paired with B-site acceptor ions), which impede domain wall motion, is increased by acceptor doping and decreased by donor doping.[19-23] Hence doping can dramatically change the piezoelectric properties, with donor dopants generally increasing the domain wall contributions and acceptors decreasing them, to produce soft and hard piezoelectrics respectively. In PZT it is accepted that the oxygen vacancy concentration is critical to determine the relative importance of the domain wall contributions to piezoelectricity. It is therefore appropriate to consider evidence for a similar mechanism in PMN-PT ceramics, whilst bearing in mind the relaxor origins of PMN-PT.

Here we report on the analysis of the dielectric, piezoelectric and conduction properties of Sm-doped PMN-PT, including Rayleigh analysis and impedance spectroscopy as a function of temperature, yielding details of the conductivity mechanisms. To gain additional insight, results of manganese (Mn) co-doping experiments are also presented. Manganese is recognised as an acceptor dopant and can reduce the loss factor and increase the mechanical quality factor Q_m.[7, 24] It is generally believed that in ferroelectric perovskites Mn doping introduces oxygen vacancies, with which it forms polar defect pairs and thereby pins the domain walls.[24]

Experimental

All samples were prepared by solid state reaction. $Pb(Mg_{1/3}Nb_{2/3})_{0.71}Ti_{0.29}O_3$ (PMN-29PT) ceramics, undoped and doped with Sm and Sm + Mn, were prepared by using the two step columbite precursor method. In order to avoid the formation of unwanted pyrochlore phase, $(MgCO_3)_4$•$Mg(OH)_2$•$5H_2O$ (Alfa Aesar, 99%) and Nb_2O_5 (Sigma-Aldrich, 99.9%) were firstly mixed in the stoichiometric ratio, then calcined at 1150°C for 4h to pre-synthesise $MgNb_2O_6$ powders. In the second stage, the precursor $MgNb_2O_6$ was mixed with PbO, TiO_2 (Sigma-Aldrich, 99.9%) and one of two dopant recipes comprising Sm_2O_3 or Sm_2O_3 and MnO_2 (Alfa Aesar, 99.99%). The doped compositions were batched assuming Pb vacancy compensation, as used by Li et al.,[11] according to $Pb_{0.9625}Sm_{0.025}(Mg_{1/3}Nb_{2/3})_{0.71}Ti_{0.29}O_3$ to form 2.5%Sm-doped samples. For the Sm-Mn co-doped sample, the composition was $Pb_{0.9625}Sm_{0.025}Mn_{0.01}[(Mg_{1/3}Nb_{2/3})_{0.71}Ti_{0.29}]_{0.99}O_3$. After ball milling and drying, the mixed powders

were calcined at 850˚C for 4h, and 1wt.% binder was added into the calcination powders. The powders were uniaxially pressed into circular discs of 10 mm diameter and 1.5 mm thickness. The pellets were sintered at 1150˚C for 2h after a binder burn out process at 600˚C for 4h. The sintered pellets were ground and polished for X-ray diffraction (XRD) analysis. Opposite surfaces of the pellets were coated with a fired-on silver paint and then heated to 550˚C for 20 mins to obtain a smooth, flat surface.

Polarization (P) and strain (x) as a function of field (E) were measured using a Precision LCII Ferroelectric Tester (Radiant Technologies Albuquerque, USA) in conjunction with an MTI 2000 Fotonic displacement sensor (MTI Instruments, Inc, Albany, USA). The relative permittivity and loss were measured upon heating using an LCR meter (HP4284) with the sample in a tube furnace. Impedance spectroscopy measurements were performed using ModuLab XM MTS (Solartron Analytical, UK) in conjunction with the tube furnace over a temperature range from 20 to 650˚C. Samples were poled at 10 kV/cm for 15 minutes at room temperature in silicon oil. After poling, the piezoelectric coefficient d_{33} was determined using the Berlincourt method.

Results

Fig. 1 shows XRD diffraction patterns of undoped and doped PMN-29PT ceramics after sintering. The undoped ceramics form as a pure perovskite phase, but the doped samples all show the existence of a secondary phase. For both Sm and Sm + Mn co-doped PMN-29PT ceramics, although a small quantity of pyrochlore phase is observed (3 to 4 vol%), the shift in perovskite peaks to a high angle indicates a decrease of lattice parameters, suggesting that the majority of the Sm dopant has entered into the A-site in the perovskite lattice. Both undoped and doped patterns are consistent with a mixture of tetragonal and rhombohedral symmetries.

The results of higher resolution XRD scans of the (200) peak for pure and Sm-doped samples in the 2θ range of 44 ~ 44.5° are shown in Supplemental Materials Fig. S1. In contrast to pure PMN-PT, the peak in Sm-doped material becomes more asymmetric, due to increased (200)/(002) splitting. The peak for Sm-doped samples can be fitted with two pseudo-Voigt peaks as shown in Fig. S1(b), implying the formation of a tetragonal phase and a shift of MPB to lower $PbTiO_3$ concentration.[10, 11]

The temperature dependence of the real and imaginary parts of relative permittivity (ε'_{33} and ε''_{33}) at different frequencies for undoped and Sm-doped PMN-29PT (represented as Sm-29PT) ceramics is shown in Fig. 2(a). Both compositions display a typical relaxor behavior. At 1 kHz, the undoped composition exhibits a peak in ε'_m of 10,810 at 132˚C. With the addition of Sm, the room

temperature value of ε'_{33} increase from 1,650 to 4,430 and the temperature of the maximum ε'_m (T_m) shifts to 85˚C with a value of 24,460. The addition of Sm also increases the room temperature value of ε''_{33} from 31 to 155 and possesses a higher maximum ε''_{33} of 1,080 at 79˚C than that of 254 at 122˚C in undoped samples. These and other measured characteristics are compared in Table I. Fig. 2(b) shows the normalized ε'_{33} and ε''_{33} at different frequencies. Within the normalized scale, it is clear that T_m is rather insensitive to frequency from 1 kHz to 100 kHz; the dispersion in T_m exhibits no large differences in these samples, which is about 2~3K.

Plotting reciprocal permittivity vs $1/T$ (as shown in Fig. S2(a) in the Supplemental Materials) allows identification of the temperature at which the high temperature permittivity departs from the Curie Weiss law, known as the Burns temperature (T_b). This decreases on Sm doping from 225 to 199˚C, whilst the Curie-Weiss temperature (T_0) decreases from 174 to 151˚C and the Curie constant (C) increases from 0.76×10^5 to 0.93×10^5. For a second order phase transition, the permittivity below T_0 is given by $C/2(T_0\text{-}T)$ and from the above values of C and T_0, ε_r at 300 K is predicted to be 246 and 353 for the undoped and Sm-doped materials, respectively.

The permittivity peak associated with relaxor-like transitions is often fitted to a phenomenological equation [25, 26]

$$\varepsilon = \frac{\varepsilon_m}{1 + ((T - T_m)/\delta)^\gamma}, \quad (1)$$

where ε_m is the maximum dielectric constant, T and T_m are the temperatures corresponding to ε and ε_m, respectively. γ is the diffuseness exponent and δ is the diffuseness parameter. The exponent $\gamma = 1$ describes the Curie-Weiss law of a normal ferroelectric phase transition and $\gamma = 2$ represents a diffuse phase transition corresponding to a classical relaxor. In general, relaxor ferroelectrics systems with an incomplete diffuse phase transition are assigned in the range of $1 < \gamma < 2$.[25-27] Fits of Eqn. (1) for undoped and Sm-doped PMN-29PT ceramics are shown in Fig. S2(b) of the Supplemental Materials. The equation fits well for both compositions in the paraelectric region ($T \geq T_m$), but for $T < T_m$, the equation fits the data of the undoped sample better than that of Sm-doped sample, with the peak for the doped sample being narrower than the fit to Eqn. (1) suggests. Moreover, γ drops from 1.99 to 1.79 and δ decreases from 37.33˚C to 35.60˚C with Sm doping. The slight decrease in both γ and δ could be interpreted as there being less disorder in the Sm-doped sample than in undoped PMN-PT. Also, in this work, T_m is relatively independent of frequency in both undoped and Sm-doped compositions, similar to that of Sm-

modified PZT.[28] A change in the relaxor-associated contribution is therefore not sufficient to explain the significant increase of dielectric permittivity in Sm-doped PMN-PT.

The results of measurements of d_{33} on poled samples using a Berlincourt meter are also tabulated in Table I. With Sm doping there is a 170% increase in d_{33} from 230 to 620 pC/N. However, with addition of Mn, d_{33} is approximately halved, suggesting that either the mechanism of Sm-doping enhancement is partly reversed, or a new mechanism inhibiting d_{33} is introduced.

The unipolar electric field-induced polarization for undoped and Sm-doped PMN-29PT ceramics with increasing field amplitude up to 9 kV/cm has been analysed. The raw data are shown in Fig. S3 of the Supplemental Materials. For the maximum field amplitude, the two samples exhibit similar maximum values of polarization, however for lower field amplitudes, the Sm-doped sample achieves larger polarizations. Expressing the ratio of maximum polarization (P_{max}) to field amplitude (E_0) as

$$\varepsilon_0 \varepsilon^* = P_{max}/E_0 \,, \qquad (2)$$

where ε_0 is dielectric permittivity of free space, and ε^* is the effective relative dielectric permittivity of the material for high fields. Fig. 3 compares ε^* as a function of E_0 for undoped and doped samples. The dependence of permittivity and piezoelectric charge coefficient on the amplitude of the probe field (E_0) is frequently employed to assess the contribution of domain wall motion in piezoelectric ceramics. For fields less than approximately half the coercive field, at which full domain switching may start to occur, a linear dependence can be observed, known as the Rayleigh law:[3, 29-34]

$$\varepsilon_r(E_0) = \varepsilon_i + \alpha E_0 \qquad (3)$$

where ε_i is said to represent the reversible, lattice and non-lattice contributions to permittivity and αE_0 is the irreversible contribution responsible for hysteresis. In conventional ferroelectrics, the non-lattice contributions are usually attributed to domain wall motion, which can be both reversible and irreversible. Soft, donor doped PZT is characterized by a large value of the Rayleigh coefficient, α, suggesting a large irreversible contribution from domain wall motion, whilst hard PZT exhibits a small value of α.[20, 22, 29]

Here, the undoped material obeys the Rayleigh law up to 4 kV/cm with a value of ε_i of 1680 (at zero field) and α = 690 cm/kV. Above 4 kV/cm, ε^* becomes approximately constant at 4500. For Sm-doped samples, the Rayleigh Law is followed up to a field amplitude of only 2 kV/cm; ε_i and α are increased by approximately a factor of 2, compared to undoped material, to

4140 and 1300 cm/kV respectively. For fields greater than 2 kV/cm, ε^* of the Sm-doped composition decreases linearly to converge on the undoped value at $E_0 \approx 10$ kV/cm.

From this analysis, Sm doping can be interpreted as enhancing both the reversible and irreversible contributions to permittivity, however the irreversible enhancement to the value α ceases above 2 kV/cm; in the conventional model, the decline in permittivity above this field would suggest that all domains have switched and saturation of the lattice contribution has occurred. This point is not reached until 4 kV/cm in undoped materials.

The ε^* of Sm+Mn-doped samples exhibits a different behaviour and can be separated into two regions with different gradients. At low field, the Rayleigh coefficient is less than that of pure PMN-PT, suggesting a reduction in the irreversible contributions such as domain wall motion. When the electric field is increased up to 3 kV/cm, an inflection point is observed and the Rayleigh coefficient increases to a value that is higher than that of undoped materials and close to that of Sm-doped ceramics, suggesting that beyond 3 kV/cm domain walls pinning is overcome and the walls then contribute to the reorientation of the polarization.

Fig. 4 shows the polarization-field (*P*-*E*) and strain-field (*x*-*E*) hysteresis loops for bipolar fields for undoped and doped samples. Compared to undoped material, the addition of Sm reduces the coercive field E_C from 4.7 to 2.8 kV/cm and slightly increases the spontaneous polarization P_s from 17.2 to 20.2 μC cm^{-2}. For Sm+Mn-doped PMN-29PT, P_s decreases to 11 μC cm^{-2}.

The induced strains for undoped and Sm-doped ceramics are consistent with the observed polarizations, but due to the quadratic relationship between strain and polarization, the comparative differences are greater. The maximum induced strain for the undoped material is 0.04%, equivalent to an electrostriction coefficient $Q = 0.0138$ m^4 C^{-2}, whilst at a slightly lower field the maximum strain for the Sm doped material is almost 0.058%, giving $Q = 0.0142$ m^4 C^{-2}. The electrostriction coefficients are considered equal within the margin of error of the measurements. On the other hand, the Sm + Mn doped sample has a maximum strain of 0.032%, which is equivalent to an electrostriction coefficient of 0.0274 m^4 C^{-2}, nearly twice that of the two other compositions.

The bulk resistance of undoped and Sm-doped PMN-29PT samples was estimated from complex impedance plots (Z' vs Z''), as the low frequency intercept on Z' axis. The temperature dependence of the DC conductivity σ for the samples is shown in Fig. 5, in the form of Arrhenius plots. All data could be fitted satisfactorily by the equation

$$\sigma = \sigma_0 \exp\left(-\frac{E_a}{k_B T}\right) \quad (4)$$

within the temperature range of ~520-900K, where σ_0 is a constant, E_a is the activation energy for conduction and k_B is the Boltzmann constant, the values of σ_0 and E_a are shown in Table I. On Sm doping, there is a slight increase of E_a from 1.30 to 1.37 eV, but a reduction in σ_0 by a factor of 27.

Discussion

In agreement with previous authors,[10, 11] it is shown here that the addition of 2.5% Sm in place of Pb in 0.71PMN-0.29PT results in a significant increase in the permittivity and piezoelectric charge coefficient. It is noted that this is accompanied by a reduction in T_m, but apparently not so much that would explain all the increase in permittivity and piezoelectric charge coefficient at room temperature. The addition of Sm does not increase either the diffuseness degree or frequency dispersion in this system. However, there is a marked increase in spontaneous polarization P_s and a significant decrease in conductivity as a result of the Sm-doping. The increase in maximum induced strain as result of Sm doping is consistent with the enhancement in P_s and an electrostriction coefficient of 0.014 m^4 C^{-2}. The impedance spectra confirmed that the decrease in conductivity could be attributed to the major phase, suggesting that the minor pyrochlore phase is not the origin of the observed changes from Sm-doping.

Nominally undoped Pb-based perovskites are often sub-stoichiometric in Pb, due to the high volatility of PbO. The loss of Pb would normally be expected to be compensated by the formation of oxygen vacancies or holes:

$$PbO \leftrightarrow PbO\uparrow + V''_{Pb} + V^{\cdot\cdot}_{O} \quad (5)$$

$$Pb^{x}_{Pb} + \frac{1}{2}O_2 \leftrightarrow PbO\uparrow + V''_{Pb} + 2h^{\cdot} \quad (6)$$

However, oxygen vacancies can also form independently, compensated by electrons:

$$O^{x}_{O} \leftrightarrow \frac{1}{2}O_2 + V^{\cdot\cdot}_{O} + 2e' \quad (7)$$

Depending on the oxygen partial pressure and the steps taken to reduce lead loss during sintering, the conductivity of Pb-based perovskites could be dominated either by oxygen vacancies and electrons or by holes. Moreover, the nominal pure materials employed to produce ceramics contain relatively high levels of impurities which may also play a role in determining the dominant charge carriers. The most common impurities are expected to be acceptors and under all but highly

oxidizing conditions,[35, 36] are expected to result in an increase in oxygen vacancy concentration, for example:

$$Na_2O \leftrightarrow 2Na'_{Pb} + O_O^x + V_O^{\cdot\cdot} \quad (8)$$

Hence, other than chemical impurities, the most likely defects in lead-based perovskites are thought to be lead and oxygen vacancies, with the latter dominating the conductivity at intermediate temperatures.

The coexistence of acceptor ions and oxygen vacancies in PZT is believed to be the origin of hard piezoelectric properties; the resulting dipolar defect pairs align with the local polarization, increasing the energy barrier for domain wall motion.[19-23] Hence, in deliberately acceptor-doped ceramics, the domain wall mobility is lower, resulting in a reduction of the domain wall contribution to the piezoelectric charge coefficient.[23, 30] Donor dopants have the opposite effect, markedly increasing the piezoelectric charge coefficients and increasing both dielectric losses and polarization hysteresis due to an increase in domain wall mobility.

Due to ion size and charge considerations, Sm^{3+} would normally be expected to substitute for Pb on the A-site of a perovskite as a donor ion. In this case, charge compensation can be achieved by electron donation/hole annihilation, by A-site vacancies or by oxygen vacancy annihilation:

A $$Sm_2O_3 \leftrightarrow 2Sm_{Pb}^{\cdot} + 2O_O^x + \frac{1}{2}O_2\uparrow + 2e' \quad (9)$$

B $$Sm_2O_3 + 2h^{\cdot} \leftrightarrow 2Sm_{Pb}^{\cdot} + 2O_O^x + \frac{1}{2}O_2\uparrow \quad (10)$$

C $$Sm_2O_3 \leftrightarrow 2Sm_{Pb}^{\cdot} + V''_{Pb} + 3O_O^x \quad (11)$$

D $$Sm_2O_3 + V_O^{\cdot\cdot} \leftrightarrow 2Sm_{Pb}^{\cdot} + 3O_O^x \quad (12)$$

Compensation through B-site vacancies is theoretically possible, but unlikely to happen, unless deliberately promoted through the formulation. If A-site vacancy compensation is dominant, then donor doping would leave the conductivity of the material unchanged compared to undoped material (mechanism C). An increase in conductivity on doping would tend to indicate that electron conduction (mechanism A) is dominant, whilst a reduction in conductivity would indicate that either hole or oxygen vacancy annihilation (B or D) is dominant.

As the samples considered here were not processed at high oxygen partial pressure, we conclude that despite having been batched to favor A-site vacancy compensation, the source of the reduction in conductivity of Sm-doped sample (Fig. 5) is oxygen vacancy annihilation. Also, the activation energy for oxygen ion conductivity in perovskites has been observed to increase with

increasing oxygen occupancy within the range from 0.5 to 2.0 eV.[37, 38] Hence both the decrease in σ_0 and small increase in E_a suggest a decrease in oxygen vacancy concentration with the addition of Sm. A comparison of the σ_0 values suggests a decrease in oxygen vacancy concentration of more than 25 times with Sm-doping. This result is consistent with that in Sm-doped PZT, which shows a reduction in conductivity and an increase in E_a with Sm doping.[39, 40] The unusual frequency dependence of ε'' for the undoped sample may also be a consequence of high conductivity, whereas the frequency dependence of the Sm-doped sample is consistent with normal relaxor behavior.

The dramatic enhancement of dielectric constant and d_{33} at room temperature and in the vicinity of T_C in Sm-doped PZT compositions is ascribed to the extrinsic contribution. The introduced Sm favors the formation of tetragonal and pseudo-cubic coexistence phase in PZT; it modifies the vacancy concentration and facilitates domain wall motion.[17, 18] This improvement of dielectric and piezoelectric response with a small addition of Sm^{3+} on A-site is also observed in some lead free piezoelectric materials, such as $BaTiO_3$,[41, 42] $BiFeO_3$,[43] $(Na_{0.5}Bi_{0.5})_{0.94}Ba_{0.06}TiO_3$ [44-46] and other systems [47, 48]. This suggests that the mechanism of at least one contribution to the enhanced properties in Sm-doped PMN-PT may not be fundamentally different from other piezoelectric materials.

The Rayleigh analysis shows that the reversible (ε_i) and irreversible contributions (αE_0) increase by factors 2.5 and 1.9 respectively with Sm doping in Fig. 3. The simplest derivation of the Rayleigh law is one in which at zero applied field the domain walls occupy minima within an energy landscape created by randomly distributed pinning defects. On the application of a given AC field, the domain walls that sit in relatively deep minima oscillate within those minima, producing a reversible contribution to the induced polarization. However, a fraction of the domain wall population will escape their zero field wells and traverse a longer distance before being trapped by deeper minima, thereby providing a larger, but irreversible contribution to the polarization. Hence, the change in polarization, ΔP, due to domain wall motion under an applied field of amplitude E_0, will be

$$\Delta P = NP_s[(1-\varphi)\mu_r + \varphi\mu_i]E_0 \qquad (13)$$

where N is the line density of domain walls, P_s is the spontaneous polarization, φ is the fraction of walls that escape the initial potential well and μ_r and μ_i are the average mobilities (distance

travelled per unit field) for the reversible and irreversible domain wall translation. If φ is linearly dependent upon the field amplitude such that $\varphi = \eta E_0$, then

$$\Delta P = NP_s[\mu_r + \eta(\mu_i - \mu_r)E_0]E_0 \quad (14)$$

and permittivity is given by

$$\varepsilon = \varepsilon_{lat} + NP_s\mu_r + 2N\eta P_s(\mu_i - \mu_r)E_0 \quad (15)$$

where ε_{lat} is the lattice contribution.

Eqn. (15) is equivalent to the Rayleigh law with $\varepsilon_i = \varepsilon_{lat} + NP_s\mu_r$ and $\alpha = 2N\eta P_s(\mu_i - \mu_r)$. Hence both terms are dependent upon the spontaneous polarization, the domain wall density and a combination of mobilities of reversible and irreversible domain walls. We note that by definition, $\mu_i > \mu_r$, so α is always positive.

Inspection of the Rayleigh analysis for a wide range of materials shows that a plot of ε_i vs α, (Fig. 6) yields an approximate linear relationship with a correlation factor of 0.85. This supports the conclusion of the above analysis that ε_i and α, are not independent terms. The slope of 2.4 suggests that ε_i is more sensitive than α to material changes, and this is also seen to be the case with Sm-doped PMN-PT. Despite the large values of ε_i and α, for the materials in the current work, they lie close to the trendline for the complete dataset in Fig. 6, suggesting that the mechanisms underlying the Rayleigh law in Sm:PMN-PT are not radically different to conventional piezoelectric materials.

Whilst there is a 15% increase in P_s on Sm-doping, this does not account for the observed increases to ε_i and α, suggesting that at least in the case of α there is either a significant increase in domain wall density or mobility. As there is only a modest change in P_s, a significant change to domain wall density would also not be expected, therefore the increase in α suggests an increase in the mobility for irreversible motion μ_i with Sm doping. This is consistent with the evidence from conductivity measurements indicating a reduction in oxygen vacancy concentration and is directly comparable to the existing models for donor doping of PZT.

It would not be inappropriate to assume that the mobility of reversible domain walls also increases, accounting for at least part of the remarkable increase in ε_i with Sm-doping. However, this cannot be the only contribution as it would probably require the increase in μ_r to exceed that in μ_i, which would be inconsistent with the positive increase in α. It is therefore proposed that the lattice contribution, ε_{lat}, also plays a significant role, as suggested by Li et al.[11] Hence, in light of

the significant decrease in conductivity, it is pertinent to consider whether the oxygen vacancy concentration can also influence ε_{lat}.

As PMN-PT is close to the MPB, indicating a rather isotropic free energy surface in polarization space, the main contribution to ε_{lat} and the corresponding contributions to the piezoelectric coefficient are understood to be polarization rotation away from the polar direction towards the direction of the applied field. Dipolar defects that have aligned with the spontaneous polarization will act to increase the anisotropy, deepening the polarization potential along this single axis and inhibiting rotation of the polarization towards the applied field direction, resulting in a reduction of the low-field permittivity and piezoelectric charge coefficient compared to defect-free materials.

To determine whether this is a feasible model, calculations have been undertaken using the Landau-Devonshire theory of ferroelectrics,[56, 57] employing the free energy coefficients determined by Zhang et al.[57] for 70PMN-30PT. The detailed calculation method is given in Supplemental Materials Fig. S4. An internal bias field, E_d, parallel to [111], is introduced to represent the influence of dipolar defects aligned to the polarization; the permittivity as a function of crystal direction is then calculated. Averaging over all orientations provides an estimate of the polycrystalline permittivity, $\bar{\varepsilon}$. For $\boldsymbol{E}_d = 0$, $\bar{\varepsilon} = 3363$, whilst for $\boldsymbol{E}_d = 2$ MV m^{-1}, $\bar{\varepsilon} = 1978$. The calculation illustrates the concept that defect dipoles can reduce the contribution of polarization rotation to the permittivity and hence the piezoelectric coefficient of PMN-PT. The difference between the permittivity with and without a dipole bias field calculated here could account for the experimentally observed differences between doped and undoped PMN-PT.

The above data and arguments suggest that dipolar defects involving oxygen vacancies are responsible for inhibiting both the intrinsic and extrinsic contributions to permittivity and piezoelectric coefficients in undoped PMN-PT and that the addition of Sm results in the reduction of oxygen vacancy concentration. It is relevant to ask which defect species associate with the oxygen vacancies to form the dipolar pairs. Whilst there are likely to be acceptor impurities present to which the oxygen vacancies are attracted, pairing with lead vacancies is also very likely; for $PbTiO_3$, first principles calculations[58] have shown that such a pairing between Pb vacancies and a vacancy in the next nearest oxygen site is likely, with the resulting dipole having the lowest energy when aligned to the spontaneous polarization. There is also a third possibility; when considering the local unit cell environment, a B-site occupied by a Mg^{2+} ion exhibits a relative charge of 2– compared to the background B-site average of 4+. Hence, oxygen vacancies may

migrate towards Mg^{2+} ions in order to maintain local stoichiometry closer to the average, thereby forming dipolar pairs. Thus, reorientable dipoles involving oxygen vacancies may exist even in high purity samples with low lead deficiency. The addition of Mn in conjunction with Sm appears to cancel the effect of Sm presumably by reintroducing oxygen vacancies.

Whilst the above arguments focus on the ease with which polarization can rotate in the weak to intermediate field range, the question of the change in magnitude of P_s with Sm doping is outstanding. It may be a purely chemical effect. Although Sm doping reduces T_C, which might to be expected to reduce value of P_s at room temperature, we propose that the increase in P_s is consistent with the significant reduction in the oxygen vacancy concentration that is observed. That is, oxygen vacancies reduce the intrinsic spontaneous polarization in their vicinity thereby diluting the macroscopic average value.

Finally, it is important to consider the potential role of oxygen vacancies and polar defect pairs on the PNR switching mechanism proposed for single crystals of PMN-PT by Li et al.[4] In this model, the large piezoelectric coefficients in PMN-PT are due to the field induced phase transformation and realignment of the polarization vector of static heterophase fluctuations that Li refers to as PNRs. It may be expected that at equilibrium, polar defect pairs within the PNRs will be aligned with the local polarization, and in a similar way to the argument made above for bulk polarization, will inhibit the reorientation of the PNRs under applied fields. Hence, the removal of polar defect pairs by Sm-doping would be expected to promote greater field-induced PNR reorientation and thereby increase the permittivity and charge coefficient. This would therefore contribute to the increase in reversible contributions in the Rayleigh law analysis, but a key question is whether such PNR switching may also result in an increase in the irreversible contributions? This is the same as asking whether this type of PNR switching is hysteretic? PNR switching can be hysteretic if either (i) the defect dipoles realign with the switching field, thereby stabilizing the new symmetry against back-switching to the original equilibrium state, or (ii) there is a significant energy barrier between the equilibrium and field aligned states which acts to trap the PNR in the new orientation after removal of the field. Case (i) seems unlikely as in PZT, it is known that the relaxation time of defect dipoles is very much longer than the period of the measurement fields. Case (ii) is certainly possible, but in materials close to an MPB such as PMN-29PT, such barriers are regarded as small and in Li's PNR model are necessarily so for the PNRs to exist. Furthermore, single crystals of these compositions for which the PNR model was proposed, are noted for their lack of dielectric and strain hysteresis, hence the proposed PNR

mechanism would be substantially anhysteretic and makes little contribution to the Rayleigh coefficient.[34] This suggests that whilst the increase in the reversible part of the permittivity can be due to enhanced PNR reorientation, the increases in irreversible contribution must be of a different origin, such as conventional ferroelastic domain wall motions, as argued above.

Conclusions

The large decrease in conductivity on doping of PMN-29PT with 2.5% Sm is attributed to a reduction in the oxygen vacancy concentration. Comparison with the correlation between reversible and irreversible contributions to permittivity of a large dataset of conventional piezoelectric materials, suggests that the Rayleigh law mechanisms of doped and undoped PMN-PT ceramics are similar to other piezoelectrics. The observed increase in the irreversible contributions on Sm-doping are consistent with an increase in the domain wall contributions to the material due to the removal of dipolar defects involving oxygen vacancies. The increase in reversible contributions can also be attributed to the reduction in the number of dipolar defects which can inhibit both bulk polarization rotation and phase switching of PNRs (heterophase fluctuations).

Given the significant potential for improvement of commercial materials, it would be of interest to attempt to control the oxygen vacancy concentration during processing without resorting to donor doping and the consequent reduction in T_C. This may also provide greater insight into the dielectric mechanisms in such materials.

Acknowledgments

This research was supported by EPSRC Grant: EP/R010293/1. Y. Li gratefully thanks the financial support from China Scholarship Council (CSC).

References

1. Cross LE. Relaxor ferroelectrics. Ferroelectrics. 1987;76(1):241-67.
2. Choi SW, Shrout TR, Jang SJ, Bhalla AS. Morphotropic phase boundary in $Pb(Mg_{1/3}Nb_{2/3})O_3$-$PbTiO_3$ system. Mater. Lett. 1989;8(6):253-55.

3. Zhang S, Li F. High performance ferroelectric relaxor-$PbTiO_3$ single crystals: Status and perspective. J. Appl. Phys. 2012;111(3):031301.

4. Li F, Zhang S, Yang T, Xu Z, Zhang N, Liu G, et al. The origin of ultrahigh piezoelectricity in relaxor-ferroelectric solid solution crystals. Nat Commun. 2016;7:13807.

5. Park S-E, Shrout T R. Ultrahigh strain and piezoelectric behavior in relaxor based ferroelectric single crystals. J. Appl. Phys. 1997;82(4):1804-11.

6. Davis M, Damjanovic D, Setter N. Electric-field-, temperature-, and stress-induced phase transitions in relaxor ferroelectric single crystals. Phys. Rev. B. 2006;73(1):014115.

7. Li Y, Yuan J, Wang D, Zhang D, Jin H, Cao M, et al. Effects of Nb,Mn doping on the Structure, Piezoelectric, and Dielectric Properties of $0.8Pb(Sn_{0.46}Ti_{0.54})O_3$-$0.2Pb(Mg_{1/3}Nb_{2/3})O_3$Piezoelectric Ceramics. J. Am. Ceram. Soc. 2013;96(11):3440-47.

8. Demathan N, Husson E, Morell A. Modification of the nanostructure and dielectric-properties of lead magnoniobate ceramics by doping. Mater. Res. Bull. 1992;27(7):867-76.

9. Cao L, Yao X, Xu Z, Feng Y. Research on dielectric and piezoelectric properties of Ta-doped $0.68Pb(Mg_{1/3}Nb_{2/3})O_3$–$0.32PbTiO_3$ ceramics. Ceram. Int. 2004;30(7):1373-76.

10. Li F, Cabral M J, Xu B, Cheng Z, Dickey E C, LeBeau J M, et al. Giant piezoelectricity of Sm-doped $Pb(Mg_{1/3}Nb_{2/3})O_3$-$PbTiO_3$ single crystals. Science. 2019;364(6437):264-68.

11. Li F, Lin D, Chen Z, Cheng Z, Wang J, Li C, et al. Ultrahigh piezoelectricity in ferroelectric ceramics by design. Nat Mater. 2018;17(4):349-54.

12. Zhong N, Xiang P, Sun D, Dong X. Effect of rare earth additives on the microstructure and dielectric properties of $0.67Pb(Mg_{1/3}Nb_{2/3})O_3$–$0.33PbTiO_3$ ceramics. Mat. Sci. Eng. B. 2005;116(2):140-45.

13. Guo Q, Li F, Xia F, Gao X, Wang P, Hao H, et al. High-Performance Sm-doped $Pb(Mg_{1/3}Nb_{2/3})O_3$-$PbZrO_3$-$PbTiO_3$-Based Piezoceramics. ACS Appl. Mater. Interfaces. 2019;11(46):43359-67.

14. Li C, Xu B, Lin D, Zhang S, Bellaiche L, Shrout T R, et al. Atomic-scale origin of ultrahigh piezoelectricity in samarium-doped PMN-PT ceramics. Phys. Rev. B. 2020;101(14):140102.

15. Kumar N, Mishra A, De A, Shankar U, Ranjan R. Factors contributing to the local polar-structural heterogeneity and ultrahigh piezoelectricity in Sm-modified $Pb(Mg_{1/3}Nb_{2/3})O_3$–$PbTiO_3$. J. Phys. D: Appl. Phys. 2020;53(16):165302.

16. Singh P, Singh S, Juneja J K, Raina KK, Pant RP, Prakash C. Effects of samarium doping on the ferroelectric properties of modified lead zirconate titanate ceramics. Integr. Ferroelectr. 2010;122(1):23-30.
17. Seshadri SB, Nolan MM, Tutuncu G, Forrester JS, Sapper E, Esteves G, et al. Unexpectedly high piezoelectricity of Sm-doped lead zirconate titanate in the Curie point region. Sci. Rep. 2018;8(1):4120.
18. Gao B, Yao Z, Lai D, Guo Q, Pan W, Hao H, et al. Unexpectedly high piezoelectric response in Sm-doped PZT ceramics beyond the morphotropic phase boundary region. J. Alloys Compd. 2020;836:155474.
19. Carl K, Hardtl KH. Electrical after-effects in Pb(Ti, Zr)O_3 ceramics. Ferroelectrics. 1977;17(1):473-86.
20. Rojac T, Drnovsek S, Bencan A, Malic B, Damjanovic D. Role of charged defects on the electrical and electromechanical properties of rhombohedral Pb(Zr,Ti)O_3 with oxygen octahedra tilts. Phys. Rev. B. 2016;93(1):014102.
21. Slouka C, Kainz T, Navickas E, Walch G, Hutter H, Reichmann K, et al. The effect of acceptor and donor doping on oxygen vacancy concentrations in lead zirconate titanate (PZT). Materials (Basel). 2016;9(11).
22. Lambeck PV, Jonker GH. The nature of domain stabilization in ferroelectric perovskites. J. Phys. Chem. Solids. 1986;47(5):453-61.
23. Morozov MI, Damjanovic D. Hardening-softening transition in Fe-doped Pb(Zr,Ti)O_3 ceramics and evolution of the third harmonic of the polarization response. J. Appl. Phys. 2008;104(3):034107.
24. Ren Z, Ye ZG. Effects of Mn-doping on PIN-PMN-PT ceramics with MPB composition. Ferroelectrics. 2014;464(1):130-35.
25. Santos IA, Eiras JA. Phenomenological description of the diffuse phase transition in ferroelectrics. J. Phys.: Condens. Matter. 2001;13(50):11733-40.
26. Mitoseriu L, Stancu A, Fedor C, Vilarinho PM. Analysis of the composition-induced transition from relaxor to ferroelectric state in $PbFe_{2/3}W_{1/3}O_3$–$PbTiO_3$ solid solutions. J. Appl. Phys. 2003;94(3):1918-25.
27. Uchino K, Nomura S. Critical exponents of the dielectric constants in diffused-phase-transition crystals. Ferroelectrics. 1982;44(1):55-61.

28. Prakash C, Thakur OP. Effects of samarium modification on the structural and dielectric properties of PLZT ceramics. Mater. Lett. 2003;57(15):2310-14.
29. Damjanovic D, Demartin M. The Rayleigh law in piezoelectric ceramics. J. Phys. D: Appl. Phys. 1996;29(7):2057-60.
30. Acosta M, Novak N, Rojas V, Patel S, Vaish R, Koruza J, et al. $BaTiO_3$-based piezoelectrics: Fundamentals, current status, and perspectives. Appl. Phys. Rev. 2017;4(4):041305.
31. Hall DA. Rayleigh behaviour and the threshold field in ferroelectric ceramics. Ferroelectrics. 1999;223(1):319-28.
32. Damjanovic D. Logarithmic frequency dependence of the piezoelectric effect due to pinning of ferroelectric-ferroelastic domain walls. Phys. Rev. B. 1997;55(2):R649-R52.
33. Bassiri-Gharb N, Fujii I, Hong E, Trolier-McKinstry S, Taylor DV, Damjanovic D. Domain wall contributions to the properties of piezoelectric thin films. J. Electroceram. 2007;19(1):49-67.
34. Li F, Zhang S, Xu Z, Wei X, Luo J, Shrout TR. Composition and phase dependence of the intrinsic and extrinsic piezoelectric activity of domain engineered (1-x)$Pb(Mg_{1/3}Nb_{2/3})O_3$-x$PbTiO_3$ crystals. J. Appl. Phys. 2010;108, 034106
35. Smyth DM. The role of impurities in insultating transition metal oxides. Prog. Solid State Chem. 1984;15(3):145-71.
36. Smyth DM. Defect structure in perovskite titanates. Curr. Opin. Solid State Mater. Sci. 1996;1(5):692-97.
37. Steinsvik S, Bugge R, Gjonnes J, Tafto J, Norby T. The defect structure of $SrTi_{1-x}Fe_xO_{3-y}$ (x = 0–0.8) investigated by electrical conductivity measurements and electron energy loss spectroscopy. J. Phys. Chem. Solids. 1997;58(6):969-76.
38. Lin GC, Liu H, Zhang JX. Oxygen Vacancy Relaxation in $Ca_3Co_4O_{9+\delta}$ Ceramics. Solid State Phenom. 2012;184:98-103.
39. Ranjan R, Kumar R, Kumar N, Behera B, Choudhary RNP. Impedance and electric modulus analysis of Sm-modified $Pb(Zr_{0.55}Ti_{0.45})_{1-x/4}O_3$ ceramics. J. Alloys Compd. 2011;509(22):6388-94.
40. Ranjan R, Kumar R, Behera B, Choudhary RNP. Effect of Sm on structural, dielectric and conductivity properties of PZT ceramics. Mater. Chem. Phys. 2009;115(1):473-77.

41. Ganguly M, Rout SK, Woo WS, Ahn CW, Kim IW. Characterization of A-site deficient samarium doped barium titanate. Physica B Condens. Matter. 2013;411:26-34.
42. Park IJ, Han YH. Effects of synthesized method on the properties of Sm-doped $BaTiO_3$. Met. Mater. Int. 2014;20(6):1157-61.
43. Wang T, Wang XL, Song SH, Ma Q. Effect of rare-earth Nd/Sm doping on the structural and multiferroic properties of $BiFeO_3$ ceramics prepared by spark plasma sintering. Ceram. Int. 2020;46(10, Part A):15228-35.
44. Fu P, Xu Z, Chu R, Li W, Zang G, Hao J. Piezoelectric, ferroelectric and dielectric properties of Sm_2O_3-doped $(Bi_{0.5}Na_{0.5})_{0.94}Ba_{0.06}TiO_3$ lead-free ceramics. Mater. Chem. Phys. 2010;124(2):1065-70.
45. Turki O, Slimani A, Seveyrat L, Sassi Z, Khemakhem H, Lebrun L. Enhancement of dielectric, piezoelectric, ferroelectric, and electrocaloric properties in slightly doped $(Na_{0.5}Bi_{0.5})_{0.94}Ba_{0.06}TiO_3$ ceramic by samarium. J. Appl. Phys. 2019;125(17):174103.
46. Xia X, Jiang X, Chen C, Jiang X, Chen Y, Tu N, et al. Enhanced piezoelectric performance and orange-red emission of Sm^{3+} doped $(Na_{1/2}Bi_{1/2})TiO_3$ based lead-free ceramics. Ceram. Int. 2017;43(1, Part A):376-84.
47. Zhang Y, Chu R, Xu Z, Hao J, Chen Q, Peng F, et al. Piezoelectric and dielectric properties of Sm_2O_3-doped $0.82Bi_{0.5}Na_{0.5}TiO_3$–$0.18Bi_{0.5}K_{0.5}TiO_3$ ceramics. J. Alloys Compd. 2010;502(2):341-45.
48. Jiao N, Xiao H, Guan L, Guo Y. Tailoring the Piezoelectric and Photoluminescence Properties of $Na_{0.5}Bi_{0.5}TiO_3$-$K_{0.5}Bi_{0.5}TiO_3$-$BaTiO_3$-Based Multifunctional Ceramics with Sm Doping. J. Electron. Mater. 2020;49(8):4923-28.
49. Krueger HHA. Stress Sensitivity of Piezoelectric Ceramics: Part 1. Sensitivity to Compressive Stress Parallel to the Polar Axis. J. Acoust. Soc. Am. 1967;42(3):636-45.
50. Li S, Cao W, Cross LE. The extrinsic nature of nonlinear behavior observed in lead zirconate titanate ferroelectric ceramic. J. Appl. Phys. 1991;69(10):7219-24.
51. Morozov M, Damjanovic D, Setter N. The nonlinearity and subswitching hysteresis in hard and soft PZT. J. Eur. Ceram. Soc. 2005;25(12):2483-86.
52. Guerra JDS, García JE, Ochoa DA, Pelaíz-Barranco A, García-Zaldívar O, Calderón-Piñar F. Interrelationship between phase transition characteristics and piezoelectric response in lead lanthanum zirconate titanate relaxor ceramics. J Mater Sci. 2012;47(15):5715-20.

53. Haugen AB, Morozov MI, Jones JL, Einarsrud MA. Rayleigh analysis of dielectric properties in textured $K_{0.5}Na_{0.5}NbO_3$ ceramics. J. Appl. Phys. 2014;116(21):214101.
54. Zhang H, Zhou J, Shen J, Jin W, Zhou J, Chen W. High-field nonlinear properties and characteristics of domain wall motion in Fe_2O_3 doped PMnS-PZN-PZT ceramics. Ferroelectrics. 2020;560(1):110-22.
55. Zheng L, Yang L, Li Y, Lu X, Huo D, Lü W, et al. Origin of improvement in mechanical quality factor in acceptor-doped relaxor-based ferroelectric single crystals. Phys. Rev. Appl. 2018;9(6):064028.
56. Haun MJ, Furman E, Jang SJ, McKinstry HA, Cross LE. Thermodynamic theory of $PbTiO_3$. J. Appl. Phys. 1987;62(8):3331-38.
57. Zhang H, Lu X, Wang R, Wang C, Zheng L, Liu Z, et al. Phase coexistence and Landau expansion parameters for a $0.7Pb(Mg_{1/3}Nb_{2/3})O_3$-$0.3PbTiO_3$ single crystal. Phys. Rev. B. 2017;96(5):054109.
58. Chandrasekaran A, Damjanovic D, Setter N, Marzari N. Defect ordering and defect--domain-wall interactions in $PbTiO_3$: A first-principles study. Phys. Rev. B. 2013;88(21):214116.

Figure Captions:

Fig. 1. XRD diffraction patterns of pure PMN-29PT and doped ceramics with addition of 2.5 mol% Sm and 2.5 mol% Sm + 1 mol% Mn after sintering at 1150°C for 2h. The perovskite phase is indexed, peaks of pyrochlore phase are marked with symbol.

Fig. 2. (a) The temperature dependence of the real and imaginary parts of permittivity and (b) the permittivity normalized to ε'_m and ε''_m for undoped and Sm-doped PMN-29PT ceramics at different frequencies.

Fig. 3. ε^* as a function of field amplitude E_0 up to 10 kV for undoped, Sm-doped and Sm+Mn doped samples, ε^* is calculated from P-E loops in Fig. S3 in the Supplemental Material.

Fig. 4. Polarization-electric (a) and strain-electric (b) hysteresis loops of undoped, Sm-doped and Sm+Mn co-doped PMN-29PT ceramics.

Fig. 5. The logarithm of conductivity σ vs. reciprocal temperature 1000/T showing linear fits to the data points.

Fig. 6. The initial permittivity, ε_i, vs Rayleigh coefficient, α, for range of materials,[31, 33, 49-55] as listed in Table SI (Supplemental Materials).

Table Captions:

Table I. Measured characteristics of the samples at 300 K and the calculated E_a at 520-900K.

Table I. Measured characteristics of the samples at 300 K and the calculated E_a at 520-900K.

Material	ε'_{33}	ε''_{33}	ε'_m	T_m	P_s	E_C	x_{max}	Q	d_{33}	ε_i	α	E_a	σ_0
				˚C	μC cm^{-2}	kV cm^{-1}	%	m^4 C^{-2}	pC N^{-1}		cm kV^{-1}	eV	S cm^{-1}
PMN-29PT	1650	31	10810	132	17.2	4.7	0.040	0.0138	230	1680	690	1.30	3361
Sm doped	4430	155	24460	85	20.2	2.8	0.058	0.0142	630	4140	1300	1.37	122.8
Sm+Mn	1800	--	11750	145	11.0	4.6	0.032	0.0274	365	1870	170/460	--	--

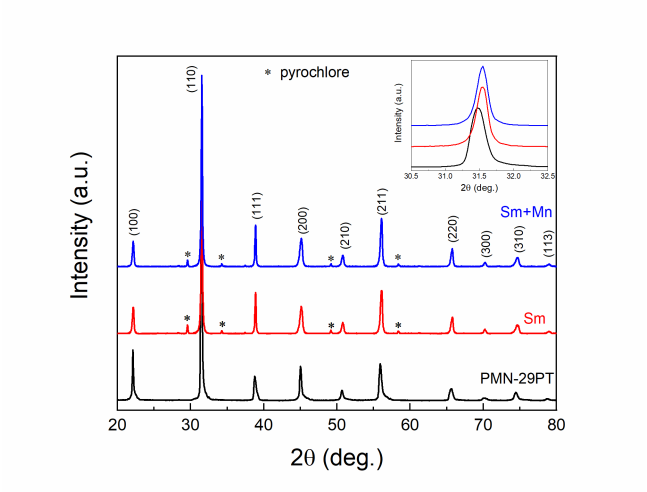

jace_17619_f1.tif

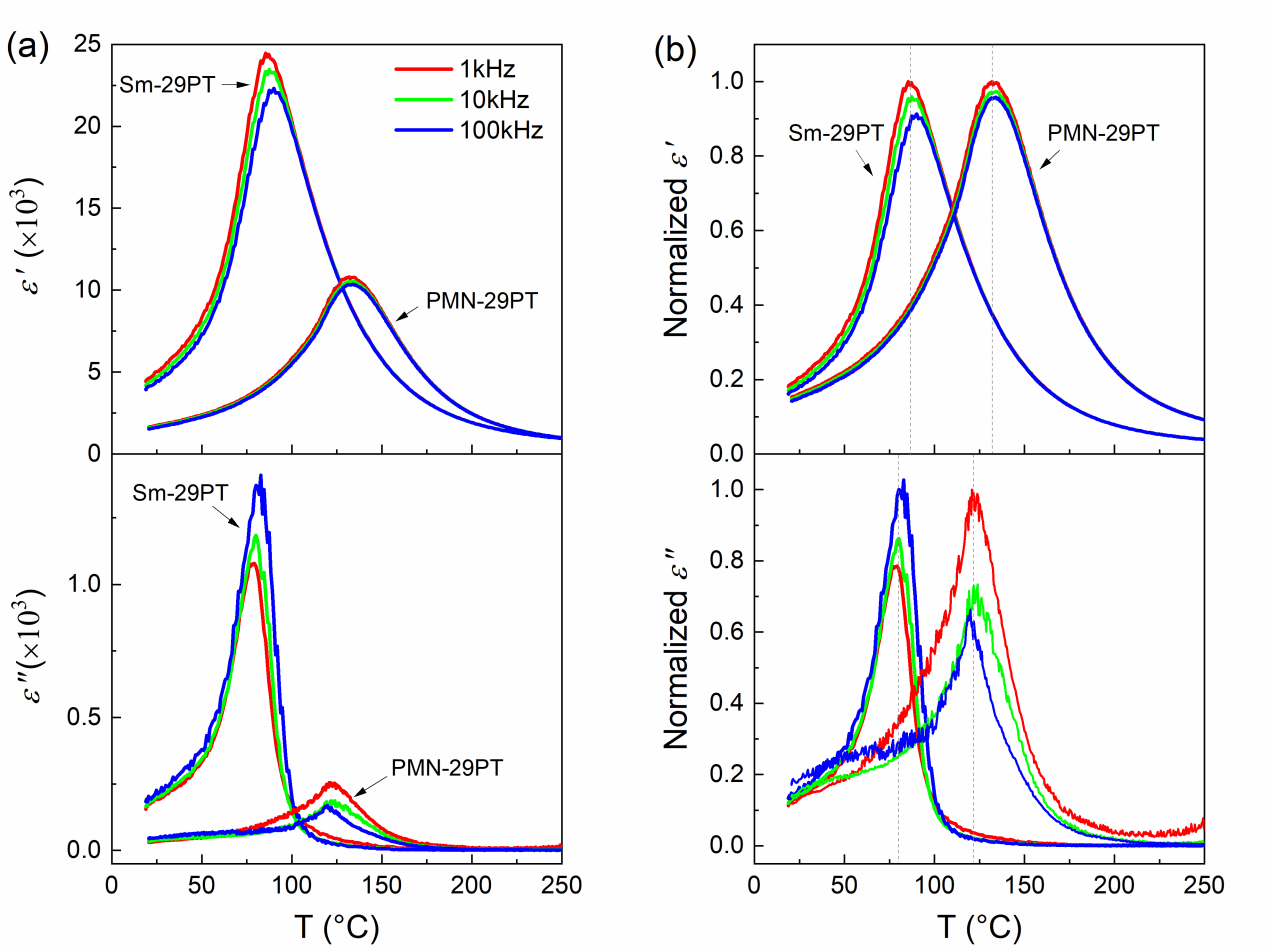

jace_17619_f2.tif

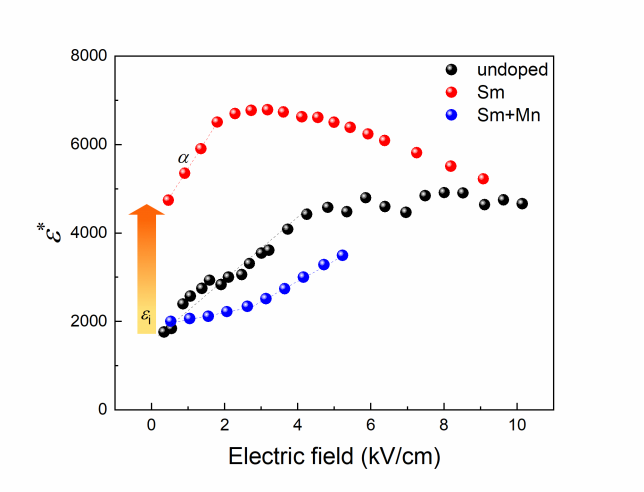

jace_17619_f3.tif

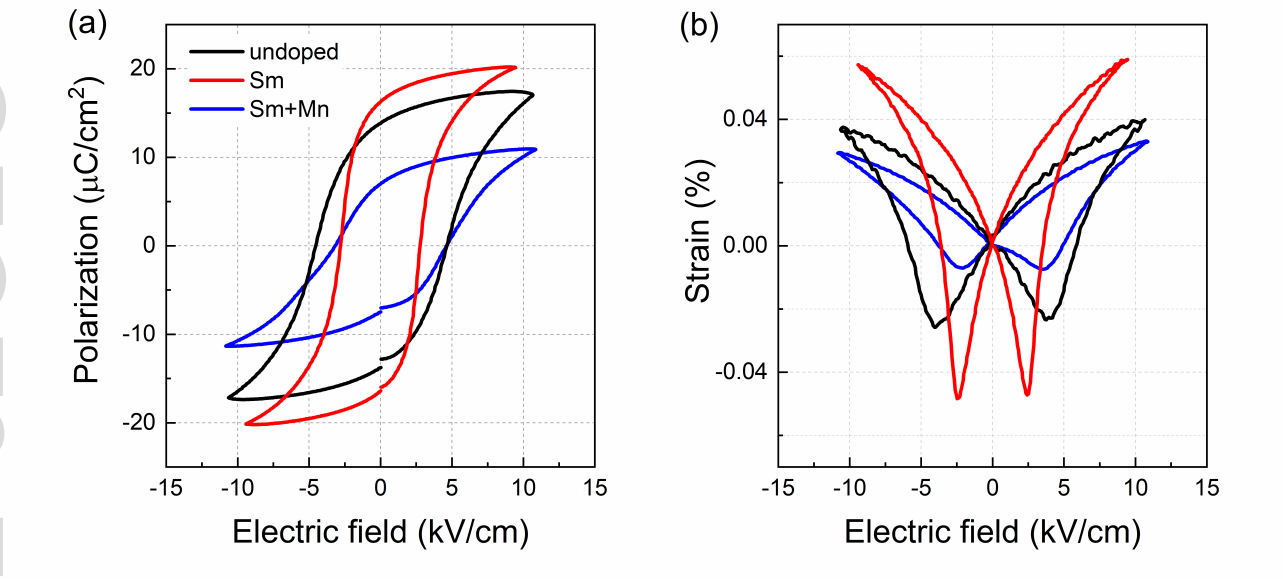

jace_17619_f4.tif

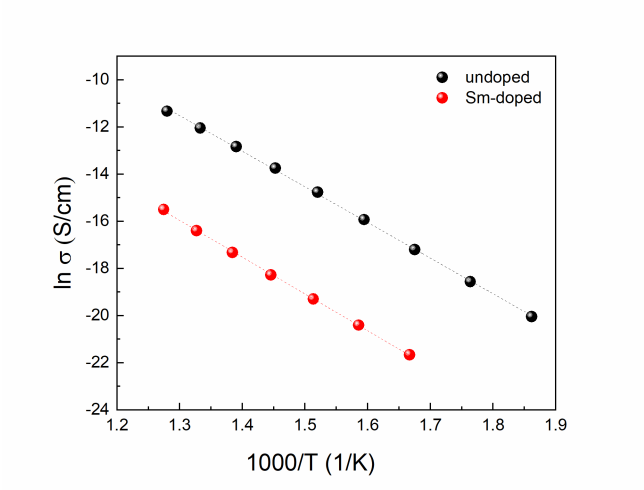

jace_17619_f5.tif

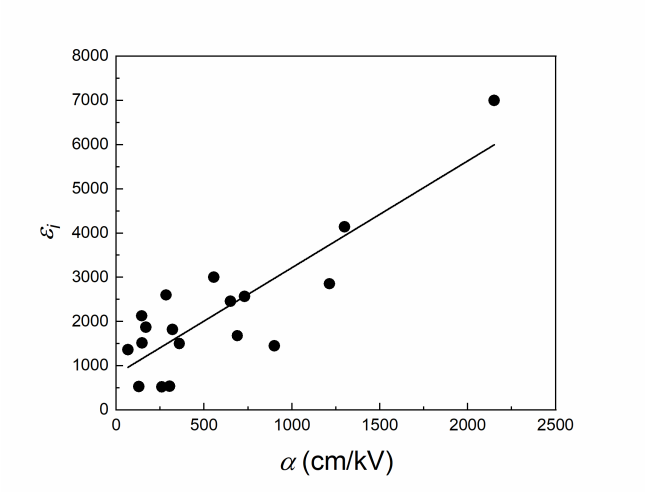

jace_17619_f6.tif